Chapter 17
Applications of Sliding Observers for FDI in Aerospace Systems

Christopher Edwards, Halim Alwi, and Prathyush P. Menon

Abstract. This chapter presents applications of second order sliding mode observer schemes to three different aerospace problems. Two relate to ADDSAFE aircraft fault detection benchmark problems. Firstly, the detection and isolation problem associated with an actuator jam/runaway is considered and secondly an actuator oscillatory failure case is tackled. For the actuator jam/runaway scenario the actuator deflection becomes decoupled from the demand issued from the flight control computer and either remains fixed at some uncommanded point or 'runs away' to an extreme value. For the OFC problem, the reconstruction scheme requires an estimate of rod speed provided by a second order sliding mode observer. Ideally low gains in the observer are required because of the noisy environment associated with the physical system. An adaption scheme is therefore required to retain sliding in the presence of severe faults. A problem associated with fault detection in a formation flying scenario, associated with satellites is also discussed. This application to a relative degree two problem would be difficult to solve using linear observer methods.

17.1 Introduction

The study of fault detection and isolation (FDI) problems has been a popular and widely researched area. One of the techniques which has gained a good deal of

Christopher Edwards
Center for Systems, Dynamics and Control, CEMPS, University of Exeter
e-mail: c.edwards@exeter.ac.uk

Halim Alwi
Control and Instrumentation Group, Department of Engineering, University of Leicester
e-mail: ha18@le.ac.uk

Prathyush P Menon
Center for Systems, Dynamics and Control, Mathematical Research Institute,
University of Exeter
e-mail: P.M.Prathyush@exeter.ac.uk

B. Bandyopadhyay et al. (Eds.): *Advances in Sliding Mode Control*, LNCIS 440, pp. 341–360.
DOI: 10.1007/978-3-642-36986-5_17

attention in recent years is sliding mode based FDI. One of the reasons is due to its robustness properties, as well as its ability to reconstruct unknown signals (faults) which may affect the system being monitored. The earliest sliding mode FDI results relied on simple residual based ideas (see for example [14, 24]). The under pinning idea in [14, 24] is to allow sliding to break in the event of a fault, and the deviation of the output estimation error away from the sliding surface indicates that a fault has occurred. In the later developments (see for example Edwards *et al* [6], Tan & Edwards [22], Jiang *et al* [15] and Kim *et al* [16]), instead of achieving detection and isolation through residuals, reconstruction of the faults has been considered. In these approaches a sliding motion is always maintained even in the presence of faults. The direct reconstruction of faults can be beneficial, especially in the case when redundancy is not available, and for sensor fault tolerant control (see for example [1]).

One of the perceived drawbacks of using sliding mode schemes in physical systems is in dealing with the discontinuities which arise from using the signum function. However there has been extensive research to obviate these difficulties ranging from simple pseudo-sliding approximations achieved through smoothing, to more advanced higher order sliding mode concepts [5, 8, 9, 17, 18, 26]. Second order sliding methods require no smoothing and allow ideal sliding motions to be achieved and therefore preserve the robustness property of sliding modes. Furthermore the inherent filtering property is beneficial for systems with noise. A recent development in second order sliding mode approaches has made a significant impression due to the inclusion of Lyapunov analysis techniques to demonstrate convergence [4, 21]. These concepts will be used in this chapter.

The Advanced Fault Diagnosis for Sustainable Flight Guidance and Control (ADDSAFE) project is a European FP7 funded consortium. The aim of ADDSAFE is to demonstrate the applicability of advanced fault detection and diagnosis (FDD) methods to support the development of sustainable aircraft. It poses challenges to improve existing FDD techniques to support new 'green' technologies allowing optimization of the aircraft structural design, improving aircraft performance and reducing the environmental footprint [19].

Two applications of 2nd order sliding mode observer schemes on the ADDSAFE aircraft benchmark problem will be presented. The first problem is associated with subtle jams and offsets in actuators which are usually automatically compensated for by the flight control system which repositions the healthy surfaces. However this can still pose a problem because drag is increased which results in excessive fuel burn. Consequently it is important to detect these incipient problems.

The second FDI problem which will be considered concerns an actuator Oscillatory Failure Case (OFC). An OFC is a type of failure in the Electrical Flight Control Systems (EFCS). When coupled with the flexible modes of the structure, OFCs can generate resonance phenomenon and cause unacceptably high vibrations and loads [10] and therefore need to be detected quickly. In the context of ADDSAFE, (as discussed in [10]) the improvement in performance of the FDI scheme allows for better optimization of the aircraft structural design, which translates to weight savings and therefore less fuel burn and a lower environmental footprint.

The final case study relates to a fault detection problem in a leader follower satellite formation situation. In the follower satellite, since the relative distance to the leader satellite is small compared to the orbit, linearizations of the Hill equations can be used to model the dynamics of the follower. These will be used as the basis of an FDI scheme to detect actuator faults in the thruster systems of the follower spacecraft. This constitutes a relative degree two problem between the measurement and the fault signals. As such traditional linear unknown input observer methods cannot be employed.

The structure of the chapter is as follows: the next section considered the applications of a sliding mode based fault detection scheme to an actuator problem; then a super twisting differentiator based scheme is used to detect the presence of oscillatory faults associated with aircraft actuators; finally a fourth order observer based on second order sliding mode principles will be developed for a specific fault detection problem in a satellite formation scenario.

17.2 Actuator Jam Problem

For this benchmark problem, a local LPV actuator model will be used for design.

17.2.1 Modeling of Hydraulic Actuator Using LPV

For the ADDSAFE benchmark problem, a LPV model representation (provided by DLR [13]), derived from the high fidelity actuator in the ADDSAFE benchmark model will be used for design. It has the form

$$\dot{x}(t) = -K(\rho)x(t) + K(\rho)u(t) \tag{17.1}$$

$$y(t) = x(t) + f_o(t) \tag{17.2}$$

where $x(t)$ represents the deflection of the actuator and $f_o(t)$ represents the additive fault in the actuator. In [13] the LPV parameters ρ chosen to describe the variation of the dynamics are

$$\rho = [\rho_1, \ldots \rho_4] := [m, X_{cg}, h, V_{cas}] \tag{17.3}$$

which represent mass (m), center of gravity in the x-direction (X_{cg}), altitude h, and conventional airspeed V_{cas}. As shown in [13], the scalar $K(\rho) > 0$ for all ρ and varies according to

$$K(\rho) = C_a(\rho) + C_b(\rho)\,\mathrm{sign}(\dot{x}(t))(x(t) + C_c(\rho)) \tag{17.4}$$

The positive scalar $C_a(\rho)$ can be interpreted as the dominant nominal gain, $C_b(\rho)$ represents the effect of deflection angle $x(t)$ and $C_c(\rho)$ represents the effect of a position offset from the trim position [13]. These coefficients have been

obtained through an affine polynomial fit to data collected on the parameter grid of $m(kg) \in [120000,\ 220000]$, $X_{cg}(\%) \in [0.21,\ 0.38]$, $h(ft) \in [0,\ 37000]$ and $V_{cas}(kt) \in [154.6,\ 176.1,\ 190.5,\ 229.6,\ 275]$. Each coefficient can be represented by

$$C_a(\rho) = C_{a,0} + C_{a,1}\rho_1 + C_{a,2}\rho_2 + C_{a,3}\rho_3 + C_{a,4}\rho_4 \tag{17.5}$$
$$C_b(\rho) = C_{b,0} + C_{b,1}\rho_1 + C_{b,2}\rho_2 + C_{b,3}\rho_3 + C_{b,4}\rho_4 \tag{17.6}$$
$$C_c(\rho) = C_{c,0} + C_{c,1}\rho_1 + C_{c,2}\rho_2 + C_{c,3}\rho_3 + C_{c,4}\rho_4 \tag{17.7}$$

17.2.2 Sliding Mode Observer

From (17.2), the fault appears at the output of the actuator model and therefore a 'sensor fault' reconstruction scheme will be employed. Consider a new state $z_f(t) \in \mathbb{R}$ which is the filtered output of $y(t)$ given by

$$\dot{z}_f(t) = -A_f z_f(t) + A_f y(t) \tag{17.8}$$

where A_f is a positive design scalar. Substituting $y(t)$ from (17.2) into (17.8) yields

$$\dot{z}_f(t) = -A_f z_f(t) + A_f x(t) + A_f f_o(t) \tag{17.9}$$

Next, augment system (17.1) and (17.9) to create a 2nd order system

$$\dot{x}_a(t) = A_a(\rho)x_a(t) + B_a(\rho)u + F_a f_o(t) \tag{17.10}$$
$$z(t) = C_a x_a(t) \tag{17.11}$$

where the augmented states $x_a(t) = \begin{bmatrix} x(t)\ z_f(t) \end{bmatrix}^{\mathrm{T}}$ and the augmented matrices

$$A_a(\rho) = \begin{bmatrix} -K(\rho) & 0 \\ A_f & -A_f \end{bmatrix},\ B_a(\rho) = \begin{bmatrix} K(\rho) \\ 0 \end{bmatrix}, \tag{17.12}$$
$$F_a = \begin{bmatrix} 0 \\ A_f \end{bmatrix},\ C_a = \begin{bmatrix} 0\ 1 \end{bmatrix}$$

For the system in (17.10), the proposed observer has the structure

$$\dot{\hat{x}}_a(t) = A_a(\rho)\hat{x}_a(t) + B_a(\rho)u - G_l e_z(t) + G_n \nu(t) \tag{17.13}$$
$$\hat{z}_f(t) = C_a \hat{x}_a(t) \tag{17.14}$$

where the output estimation error $e_z(t) = \hat{z}_f(t) - z_f(t)$. The design parameters $G_l(\rho), G_n(\rho) \in \mathbb{R}^{2\times 1}$ are the observer gains and $\nu(t)$ is the nonlinear term used to induce the sliding motion. Consider an error $e_a = \hat{x}_a - x_a$ then subtracting (17.10) from (17.13) yields

$$\dot{e}_a(t) = A_a(\rho)e_a(t) - G_l e_z(t) + G_n \nu(t) - F_a f_o(t) \tag{17.15}$$

The objective is to force $e_z(t)$ to zero in finite time, in order to achieve a sliding mode on $\mathscr{S}_{act} = \{e_a \in \mathbb{R}^2 : e_z = 0\}$. Here the observer gains are chosen as

$$G_n = \begin{bmatrix} 0 \\ 1 \end{bmatrix} \quad G_l = \begin{bmatrix} 0 \\ -A_f + k_2 \end{bmatrix} \tag{17.16}$$

where k_2 is a chosen positive scalar. Substituting (17.16) into (17.15) the error system can be written in expended form as

$$\begin{bmatrix} \dot{e}_x(t) \\ \dot{e}_z(t) \end{bmatrix} = \begin{bmatrix} -K(\rho) & 0 \\ A_f & -k_2 \end{bmatrix} \begin{bmatrix} e_x(t) \\ e_z(t) \end{bmatrix} + \begin{bmatrix} 0 \\ 1 \end{bmatrix} \nu(t) - \begin{bmatrix} 0 \\ A_f \end{bmatrix} f_o(t) \tag{17.17}$$

From (17.17) the reduced order sliding motion is given by

$$\dot{e}_x(t) = -K(\rho) e_x \tag{17.18}$$

Since $K(\rho) > 0$ for all ρ [[13]], the reduced order sliding motion is stable and $e_x \to 0$ as $t \to 0$. From the lower equation in (17.17)

$$\dot{e}_z(t) = A_f e_x - k_2 e_z(t) + \nu(t) - A_f f_o(t) \tag{17.19}$$

During sliding $e_z = \dot{e}_z = 0$ and since $e_x(t) \to 0$, equation (17.19) reduces to

$$\nu(t) = A_f f_o(t) \tag{17.20}$$

Rearranging (17.20) an estimation of the fault is obtained as

$$\hat{f}_o(t) = A_f^{-1} \nu(t) \tag{17.21}$$

which can be reconstructed online. The nonlinear injection term $\nu(t)$ has the super twisting form

$$\nu(t) = -k_1 \operatorname{sign}(e_z(t)) |e_z(t)|^{1/2} + z(t) \tag{17.22}$$

$$\dot{z}(t) = -k_3 \operatorname{sign}(e_z(t)) - k_4 e_z(t) \tag{17.23}$$

The scalars k_1, k_3, k_4 are design freedom to be chosen. Note that (17.22)-(17.23) has a similar structure to the one in [[21]]. For a sufficiently large scalar $\varepsilon > |\dot{f}_o(t)|$, if the gains from (17.22) and (17.23) are chosen as

$$k_1 > 2\sqrt{\varepsilon} \tag{17.24}$$

$$k_3 > \varepsilon \tag{17.25}$$

$$k_4 > \frac{k_2^2 \left(k_1^3 + \frac{5}{4} k_1^2 + \frac{5}{2}(k_3 - \varepsilon)\right)}{k_1 (k_3 - \varepsilon)} \tag{17.26}$$

then $e_z(t) = \dot{e}_z(t) = 0$ in finite time [[21]].

17.2.3 Simulation

The scalar A_f which defines the output filter from (17.9) has been chosen as $A_f = 0.5$. The supertwist gains from (17.24)-(17.26) have been chosen as $k_1 = 6.6408, k_2 = 0.1, k_3 = 20, k_4 = 0.3279$.

The scheme proposed above has been tested on the nonlinear high fidelity ADDSAFE benchmark model [[11]]. The simulations are conducted at an altitude of 37000ft, a speed of 2267kts, a weight of 185 tonnes and center of gravity of 28% MAC. Figure 17.1 shows the results from a right elevator jam during a coordinated turn manoeuvre. Figure 1(b) shows that the right elevator jam which does not respond to the command signal. Figures 1(c) shows that sliding is being maintained despite the presence of the fault. Figure 1(c) also shows good reconstruction of the fault.

17.3 OFC Problem

In this section, an adaptive second order sliding mode observer algorithm will be used to estimate an actuator oscillatory failure case. The idea is to manipulate the analytical mathematical nonlinear model of the actuator to obtain an expression for the OFC signal. Most of the parameters used in the manipulated nonlinear equation are available, except for the actuator rod speed which will be supplied by the adaptive observer.

17.3.1 Modeling of Hydraulic Actuator

The hydraulic actuator model from [[10]] is given by

$$\dot{x}(t) = V_c(t)\left(\frac{\Delta_p(t) - \text{sign}(i(t))\frac{F_{aero}(t)}{S}}{\Delta_{p_{ref}} + \frac{K_d(t)}{S}V_c^2(t)}\right)^{\frac{1}{2}} \tag{17.27}$$

where nominally

$$V_c(t) = K_c i(t) \tag{17.28}$$

and K_c is a conversion factor from electrical current (mA) to speed (mm/s). The current $i(t)$ is given by

$$i(t) = K(u(t) - x(t)) \tag{17.29}$$

where K is the (fixed) servo control gain. The signal $x(t)$ is the hydraulic actuator rod position and $u(t)$ is the commanded rod position (from the FCC). The fixed constants are $\Delta_{p_{ref}}$ which is the differential pressure corresponding to the maximum

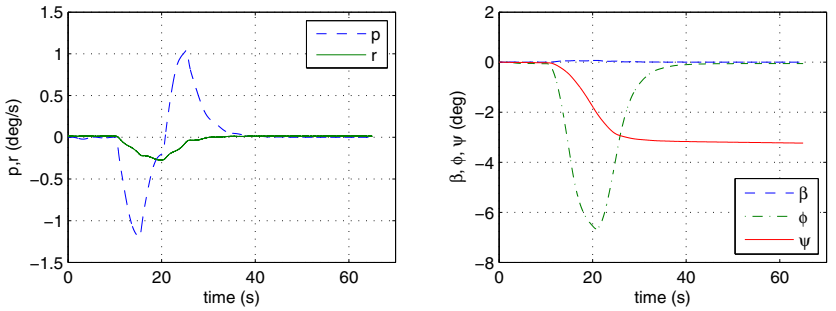

(a) states

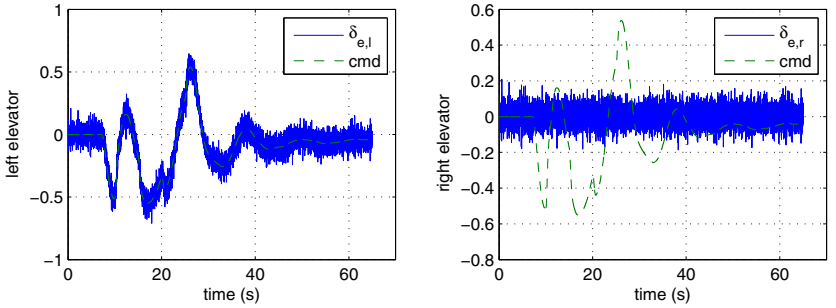

(b) elevator deflections

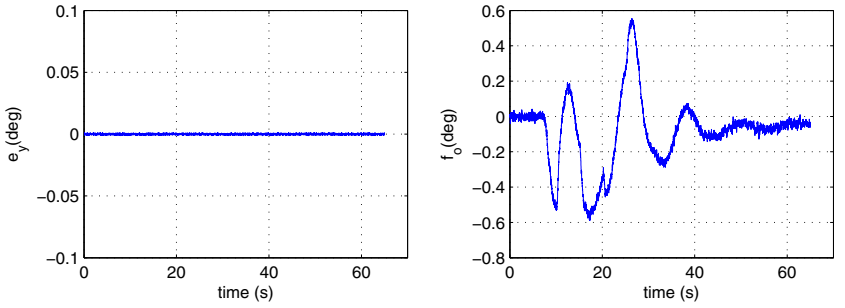

(c) e_y and fault estimations

Fig. 17.1 Turn coordination: right elevator jam

rod speed[1], and S which is piston surface area. The parameters which depend on varying operational conditions (e.g. fluid temperature and/or the number of actuators used simultaneously on a given hydraulic circuit) are: $\Delta_p(t)$ which is the actual hydraulic pressure delivered to the actuator, $F_{aero}(t)$ which is the estimate of the

[1] Maximum rod speed is achieved when the servo valve is fully open and $\Delta_p(t) = \Delta_{p_{ref}}$ [10].

aerodynamic forces applied on the control surface and $K_d(t)$ which is the adjacent actuator damping coefficient (in the case of two actuators per control surface).

17.3.2 OFC Modeling

An OFC is caused by faults in any digital component (which generate unwanted sinusoidal signals) in the actuator control loop between the FCC and the control surface. These oscillations consequently propagate within the loop [[10]]. As in [[10]], only an OFC located in the servo control loop is considered. Specifically, it is assumed that the OFC source is in the analogic output signal between the FCC and the actuator (See Figure 17.2 below). In the ADDSAFE model, the OFC affects the computed/desired rod speed $V_c(t)$ so that

$$V_c(t) = \begin{cases} V_0(t) & \text{nominal} \\ V_0(t) + K_c f_{liq}(t) & \text{liquid OFC} \\ K_c f_{sol}(t) \text{ i.e. } V_0(t) = 0 & \text{solid OFC} \end{cases} \tag{17.30}$$

where

$$V_0(t) = K_c K(u(t) - x(t)) \tag{17.31}$$

As in [[10]], the OFC signals are considered as sinusoids with amplitude and frequency uniformly distributed over the range of 1-10Hz. Beyond 10Hz, the OFC has no effect on control surface oscillation due to the low pass characteristics of the actuator. As shown in (17.30) the liquid OFC behaves as an additive fault, and the OFC signal adds to the desired position from the FCC and hence the control surface tracks the corrupted demand signal. Equation (17.30) shows that for the case of solid OFCs, the demanded surface position is replaced totally by the OFC signal. In this case, the control surface is totally 'disconnected' from the FCC and does not respond to the commanded rod position, but instead behaves as a pure periodic motion. Any attempt to damp the oscillation does not have any impact as the control surface is 'disconnected' from any demand signal from the FCC [[3, 10]].

17.3.3 OFC Estimation

Consider equation (17.27) as a special case of the differential equation

$$\dot{x}(t) = g(t,x) \tag{17.32}$$

with measured output $y(t) = x(t)$. Assume that the time derivative of the function on the right hand side of (17.32) is bounded i.e.,

$$|\dot{g}(t,x)| \leq \delta \tag{17.33}$$

for some unknown constant $\delta > 0$.

Consider an observer with the following structure

$$\dot{z}_1(t) = -\kappa_1(t)|e_1(t)|^{1/2}\ \mathrm{sign}(e_1(t)) + z_2(t) \tag{17.34}$$
$$\dot{z}_2(t) = -\kappa_2(t)\ \mathrm{sign}(e_1(t)) \tag{17.35}$$

where $e_1(t) = z_1(t) - x(t)$. Subtracting (17.32) from (17.34) yields the error system

$$\dot{e}_1(t) = -\kappa_1(t)|e_1(t)|^{1/2}\ \mathrm{sign}(e_1(t)) + z_2(t) - g(t,x) \tag{17.36}$$
$$\dot{z}_2(t) = -\kappa_2(t)\ \mathrm{sign}(e_1(t)) \tag{17.37}$$

Consider $e_2(t) = z_2(t) - g(t,x)$, then (17.36)-(17.37) can be written as

$$\dot{e}_1(t) = -\kappa_1(t)|e_1(t)|^{1/2}\ \mathrm{sign}(e_1(t)) + e_2(t) \tag{17.38}$$
$$\dot{e}_2(t) = -\kappa_2(t)\ \mathrm{sign}(e_1(t)) - \dot{g}(t,x) \tag{17.39}$$

If a 2nd order sliding motion is induced, $e_1(t) = \dot{e}_1(t) = 0$, and therefore from (17.38), $e_2(t) = 0 \Rightarrow z_2(t) = g(t,x) = \dot{x}(t)$ and therefore $z_2(t)$ from (17.35) provides an estimate of rod speed $\dot{x}(t)$. Since both $x(t)$ and $\dot{x}(t)$ are known, under the three different conditions in (17.30), equation (17.27) can be rearranged to obtain an expression for the OFC. *For the liquid OFC case*

$$f_{liq}(t) = \frac{z_2(t)f(t) - V_0(t)}{K_c} \tag{17.40}$$

where

$$f(t) = \left(\frac{\Delta_{p_{ref}}}{\Delta_p(t) - \mathrm{sign}(i(t))\frac{F_{aero}(t)}{S} - z_2^2(t)\frac{K_d(t)}{S}}\right)^{\frac{1}{2}} \tag{17.41}$$

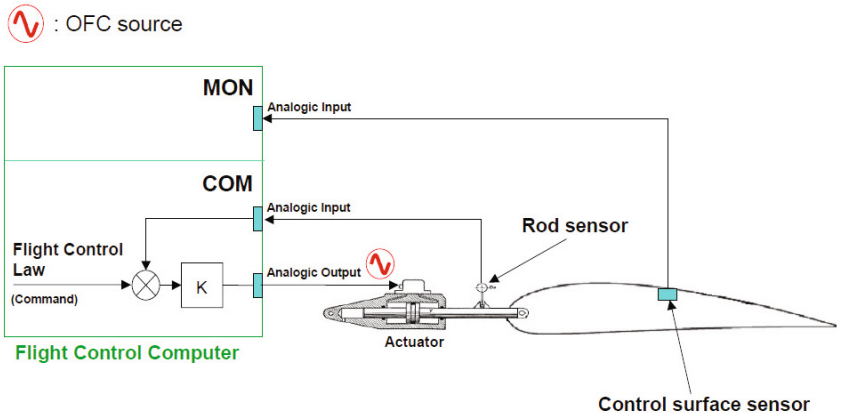

Fig. 17.2 Source of OFC in the servo control loop [10]

All the variables on the right hand side of (17.40) are available (i.e., measured or assumed to be fixed) except for the actuator rod speed. *For the solid OFC case*, since $V_0 = 0$ in (17.30), similar arguments give the estimate of the solid OFC as

$$f_{sol}(t) = \frac{z_2(t) f(t)}{K_c} \tag{17.42}$$

Here, the gains $\kappa_1(t)$ and $\kappa_2(t)$ are chosen as:

$$\kappa_1(t) = \sqrt{2\Gamma(t)} \tag{17.43}$$

$$\kappa_2(t) = 4\Gamma(t) \tag{17.44}$$

for some time varying scalar

$$\Gamma(t) = r(t) + \ell \tag{17.45}$$

where the variable ℓ is a fixed positive scalar while the varying $r(t)$ (also positive) is adapted based on the law

$$\dot{r}(t) = \begin{cases} \gamma D(|e_1(t)|^{1/2}) & \text{if } r(t) \leq r_{max} \\ 0 & \text{otherwise} \end{cases} \tag{17.46}$$

where $\gamma > 0$ is a positive design constant and the scalar $r_{max} \gg \delta$. The function $D(z) : \mathbb{R} \mapsto \mathbb{R}$ is the dead-zone function

$$D(z) = \begin{cases} 0 \text{ if } |z| < \varepsilon \\ z \text{ otherwise} \end{cases}$$

and ε is a positive scalar. The idea here is to adapt the gains when $|e_1(t)|^{1/2}$ unacceptably deviates from zero. The gain $r(t)$ will increase in magnitude according to (17.46) to force $e_1(t)$ back into a sliding regime.

The choice of $\gamma, \varepsilon, \ell$ depend on the system requirements and therefore require some design iteration. The gain ℓ represents the nominal gain when adaptation is not required, whilst γ will influence how fast the adaptive gain $r(t)$ increases. The parameter ε dictates the sensitivity of $r(t)$ to changes in $e_1(t)$ and is set to be small.

Proposition 17.1. *Using the adaptation rule (17.46) ensures the error system given in equations (17.38)-(17.39) and $r(t)$ remains bounded, and a pseudo 2nd order sliding motion is achieved in finite time forcing both e_1 and $\dot{e}_1$ to be small (depending on the choice of ε).*

Proof: See [[2]].

17.3.4 Simulations

The scheme above has been tested on the nonlinear high fidelity ADDSAFE benchmark model provided by AIRBUS [[12]]. The simulations are conducted at an altitude of 30000ft, Mach 0.64 (241kts), a weight of 200 tonnes and center of gravity of 30% MAC. In the benchmark model, the actuators are represented as high fidelity nonlinear models with parameters Δ_p, F_{aero} and K_d which vary based on changes in the operational conditions. For the observer design, these parameters are assumed to be fixed at constant values. Here, the control surface considered is the right inboard aileron. The design parameters from (17.45) and (17.46) used in the simulation are $\gamma = 3 \times 10^6$, $\ell = 50$ and $\varepsilon = 0.6$.

17.3.4.1 Simulation Results

Various OFC amplitudes and frequencies have been tested. For consistency and for comparison, all the tests were conducted using the same manoeuvre (a pilot longitudinal stick doublet input). For all tests, the OFC occurs at 10sec. For brevity, the results shown here represent the extreme cases of low and high amplitude and low and high frequency, to highlight the performance of the proposed scheme. The low amplitude case shows the smallest amplitude the scheme can detect, especially when masked by the noise in the system. The high frequency OFC case represents a challenge to detect the failure within the required time.

17.3.4.2 Solid OFC

Figure 17.3 shows an OFC of amplitude 0.5deg at a frequency of 0.5Hz. Figure 3(a) shows the effect of the OFC on the left elevator. Here, the OFC signal (blue solid line) totally replaces the commanded signal (red dashed line) and the elevator does not respond to the command signal from the FCC.

Figure 3(b) shows that there is no supertwist gain adaptation required for this level of OFC. Figure 3(c) shows both the estimated rod speed and the OFC. Here, again a good estimate of the rod speed is obtained as the estimate (blue solid line) overlaps the actual (red dashed line) rod speed. Subsequently, the good rod speed estimate provides a good OFC estimate.

17.3.4.3 Liquid OFC

Figure 17.4 shows the results for a liquid OFC with amplitude 1deg and a frequency of 7Hz. Due to the high frequency of the OFC, zoomed-in plots from 9-12sec are presented. Figure 4(b) shows that when the OFC occurs, the quality of sliding degrades and the gain $\Gamma(t)$ increases to regain sliding. Figure 4(c) shows the estimate of both the rod speed and the OFC. Again, during the period of sliding degradation, the rod speed and the OFC estimate slightly degrade, but quickly recover to provide

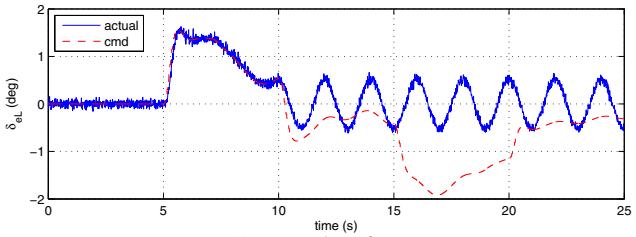

(a) control surface

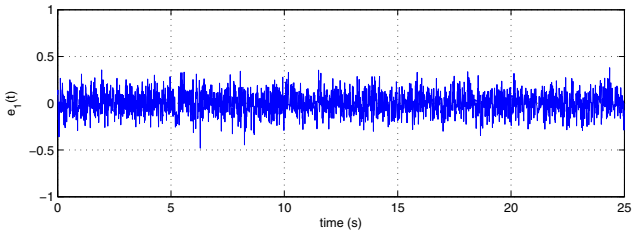

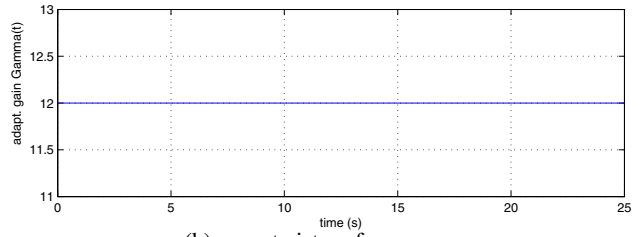

(b) supertwist performance

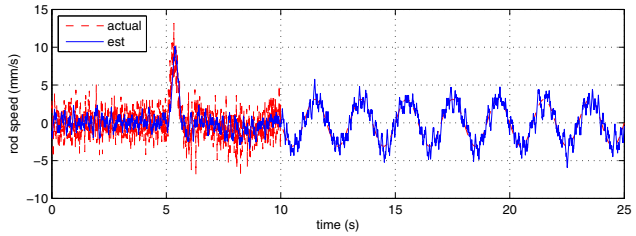

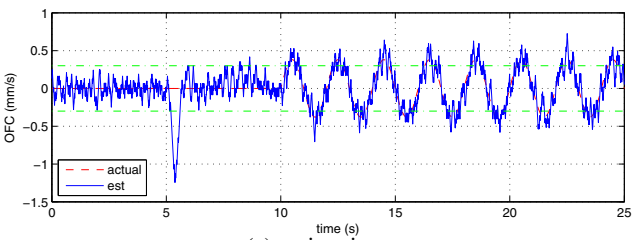

(c) estimations

Fig. 17.3 Solid OFC (amplitude 0.5, frequency 0.5)

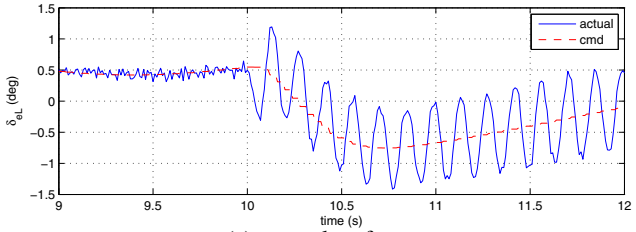

(a) control surface

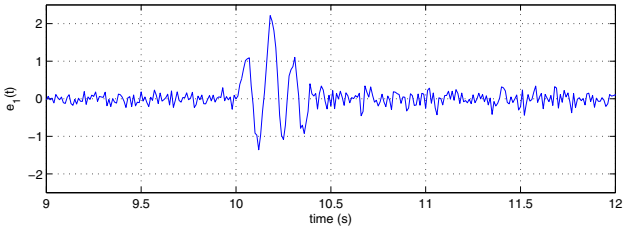

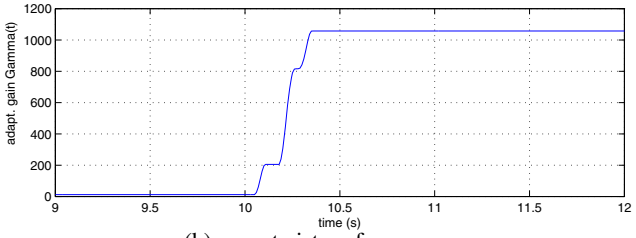

(b) supertwist performance

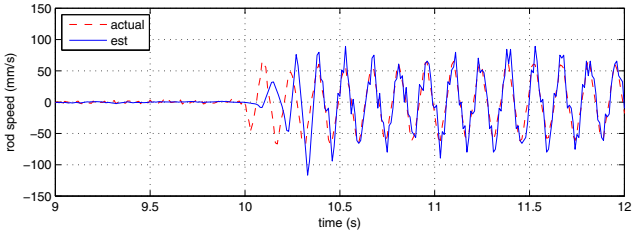

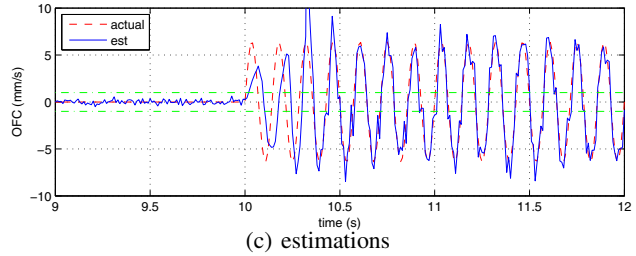

(c) estimations

Fig. 17.4 Liquid OFC (amplitude 1.0, frequency 7.0)

a good estimate once the gain $\Gamma(t)$ is sufficiently big. After adaptation of the supertwist gains, both the rod speed and the OFC estimate (blue solid line) provide a good estimate of the actual rod speed and the OFC (red dashed line).

17.4 An Observer Design for a Leader/Follower Satellite Formation

In this section a cluster of $N+1$ identical satellites, consisting of a leader satellite and N follower satellites, which are in nearby orbits, is considered. The leader satellite is on a circular Keplerian orbit and the follower satellites can measure the relative distance between all the nearby satellites as well as the leader satellite. The coupling effect between the attitude and translational dynamics of the satellites is assumed to be weak and is ignored. Also it is assumed the follower satellites have information about the control forces employed by the leader.

Since the distances between the satellites are small when compared to the diameter of the actual orbit, the relative dynamics of the i^{th} follower satellite can be studied using Hill's equations [[25]]. In general, Hill's equations consist of relative dynamics in the radial, tangential and out-of-plane direction. Only the radial and tangential $(x-y)$ plane dynamics, which are coupled, is addressed in here. The Hill equations representing the dynamics in the $(x-y)$ plane can be written as:

$$\ddot{x}_i - 2\dot{y}_i - 3x_i = u_{xi} + f_{xi} \tag{17.47}$$

$$\ddot{y}_i + 2\dot{x}_i = u_{yi} + f_{yi} \tag{17.48}$$

where x_i and y_i represent the displacements in the radial and tangential directions respectively with respect to the leader satellite, which performs a circular orbit at an angular speed of ω_n. Note that (17.47) -(17.48) have been normalized with respect to time, and have no visible dependency on ω_n as written [[20, 25]]. The control signals u_{xi} and u_{yi} are the net specific control forces, in the radial and tangential plane respectively, acting on the i^{th} follower. These are relative with respect to the leader and can be written as

$$u_{xi} = u^f_{xi} - u^l_{xi} \tag{17.49}$$

$$u_{yi} = u^f_{yi} - u^l_{yi} \tag{17.50}$$

where the superscripts f and l indicate the follower and leader respectively, and so for example, u^f_{xi} is the control signal applied to the i^{th} follower satellite in the radial direction. The terms f_{xi} and f_{yi} represent possible actuator faults. For the remainder of this section the use of the subscript i to denote the ith follower will be dropped. Since all the followers are identical, there is no ambiguity in the absence of the subcript i.

To this end, for a typical follower satellite let

$$X = (x_1, x_2, x_3, x_4) = (x, \dot{x}, y, \dot{y}) \tag{17.51}$$

The nonlinear observer which is proposed here has its roots in the second order super twisting observer proposed in [7, 8, 21]. It will be designed to simultaneously robustly estimate the states and the unknown faults, $f = \text{col}(f_x, f_y)$, from the measured relative position outputs (x_1, x_3) in each follower satellite.

Let the state estimate of the satellite be $\tilde{X} := \text{col}(\tilde{x}_1, \tilde{x}_2, \tilde{x}_3, \tilde{x}_4)$. Consider the nonlinear observer dynamical system described by

$$\dot{\tilde{x}}_1 = \tilde{x}_2 - \tilde{k}_1 |e_1|^{\frac{1}{2}} \text{sign}(e_1) \tag{17.52}$$

$$\dot{\tilde{x}}_2 = 3\tilde{x}_1 + 2\tilde{x}_4 - \tilde{k}_3 \text{sign}(e_1) - \tilde{k}_2 |e_3|^{\frac{1}{2}} \text{sign}(e_3) + u_x \tag{17.53}$$

$$\dot{\tilde{x}}_3 = \tilde{x}_4 - \tilde{k}_2 |e_3|^{\frac{1}{2}} \text{sign}(e_3) \tag{17.54}$$

$$\dot{\tilde{x}}_4 = -2\tilde{x}_2 - \tilde{k}_4 \text{sign}(e_3) + \tilde{k}_1 |e_1|^{\frac{1}{2}} \text{sign}(e_1) + u_y \tag{17.55}$$

where: $e = \tilde{X} - X$, such that $e = \text{col}(e_1, e_2, e_3, e_4)$. The $\tilde{k}_i \in \mathbb{R}^+$, $i = 1, \ldots, 4$ represent the positive design scalar gains to be determined. This will be discussed in the sequel. When compared to the classical super-twisting observer proposed in [8], additional significant cross coupling terms $-\tilde{k}_2 |e_3|^{\frac{1}{2}} \text{sign}(e_3)$ and $+\tilde{k}_1 |e_1|^{\frac{1}{2}} \text{sign}(e_1)$ are present in (17.53) and (17.55). Furthermore the skew symmetry in the coupling of the states in the satellite dynamics is exploited in proposing the new nonlinear observer. The proposed nonlinear observer will be analyzed making use of the class of Lyapunov function originally proposed in [21].

The error in the state estimate of the satellite is

$$\dot{e}_1 = -\tilde{k}_1 |e_1|^{\frac{1}{2}} \text{sign}(e_1) + e_2 \tag{17.56}$$

$$\dot{e}_2 = 3e_1 + 2e_4 - \tilde{k}_3 \text{sign}(e_1) - \tilde{k}_2 |e_3|^{\frac{1}{2}} \text{sign}(e_3) - f_x \tag{17.57}$$

$$\dot{e}_3 = -\tilde{k}_2 |e_3|^{\frac{1}{2}} \text{sign}(e_3) + e_4 \tag{17.58}$$

$$\dot{e}_4 = -2e_2 - \tilde{k}_4 \text{sign}(e_3) + \tilde{k}_1 |e_1|^{\frac{1}{2}} \text{sign}(e_1) - f_y \tag{17.59}$$

The proposed design ensures the convergence of the error dynamics associated with the estimates of the states to zero *in finite time*.

It is assumed that the unknown faults f_x and f_y in the error dynamics satisfy a-priori known upper bounds. Specifically suppose $|f_x| \leq \delta_1$ and $|f_y| \leq \delta_2$ for known constants $\delta_1, \delta_2 \geq 0$. This assumption is similar to the one made in [20, 25].

Consider a candidate Lyapunov function $V(e)$ for the error dynamics system in (17.56) - (17.59), which is inspired by the one in [21] given by:

$$\begin{aligned} V(e) = {} & 2\tilde{k}_3 |e_1| + \frac{1}{2} e_2^2 + \frac{1}{2} (\tilde{k}_1 |e_1|^{\frac{1}{2}} \text{sign}(e_1) - e_2)^2 \\ & + 2\tilde{k}_4 |e_3| + \frac{1}{2} e_4^2 + \frac{1}{2} (\tilde{k}_2 |e_3|^{\frac{1}{2}} \text{sign}(e_3) - e_4)^2 \end{aligned} \tag{17.60}$$

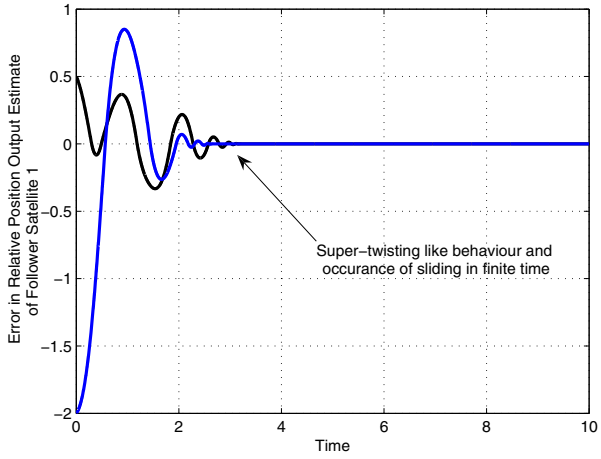

Fig. 17.5 Output estimatation errors

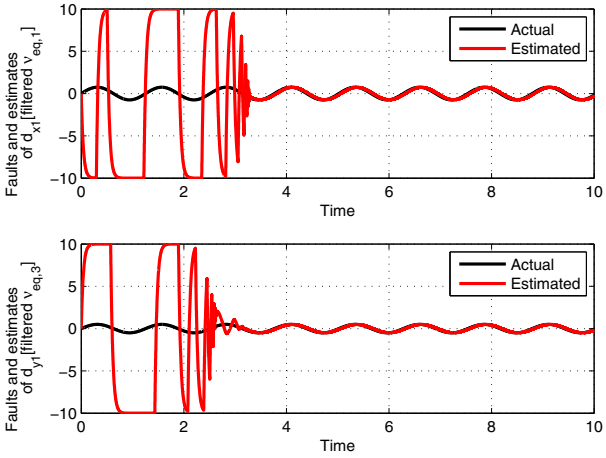

Fig. 17.6 Estimates in disturbances

For simplicity, the proposed candidate Lyapunov function can be written as a quadratic form $V(\xi) = \xi^{\mathrm{T}} P \xi$ where $\xi := \mathrm{col}(\xi_1, \xi_2)$ and $\xi_1 := \mathrm{col}(|e_1|^{\frac{1}{2}} \mathrm{sign}(e_1),\ e_2)$ and $\xi_2 := \mathrm{col}(|e_3|^{\frac{1}{2}} \mathrm{sign}(e_3),\ e_4)$. The block diagonal Lyapunov matrix

$$P = \begin{bmatrix} P_1 & \mathbf{0}_{2\times 2} \\ \mathbf{0}_{2\times 2} & P_2 \end{bmatrix} \tag{17.61}$$

where

$$P_1 = \frac{1}{2}\begin{bmatrix} 4\tilde{k}_3 + \tilde{k}_1^2 & -\tilde{k}_1 \\ -\tilde{k}_1 & 2 \end{bmatrix},\ P_2 = \frac{1}{2}\begin{bmatrix} 4\tilde{k}_4 + \tilde{k}_2^2 & -\tilde{k}_2 \\ -\tilde{k}_2 & 2 \end{bmatrix}$$

is radially unbounded if $\tilde{k}_3 > 0$ and $\tilde{k}_4 > 0$. It can be shown that the time derivative of $V(\xi)$ along the trajectories of the system (17.56) - (17.59) is given by

$$\dot{V}(\xi) \leq -\frac{1}{|e_1|^{\frac{1}{2}}}\xi_1^{\mathrm{T}}\tilde{Q}_1\xi_1 - \frac{1}{|e_3|^{\frac{1}{2}}}\xi_2^{\mathrm{T}}\tilde{Q}_2\xi_2 \tag{17.62}$$

where

$$\tilde{Q}_1 = \frac{\tilde{k}_1}{2}\begin{bmatrix} 2\tilde{k}_3 + \tilde{k}_1^2 - 2\delta_1 & -\tilde{k}_1 - 2\frac{\delta_1}{\tilde{k}_1} \\ -\tilde{k}_1 - 2\frac{\delta_1}{\tilde{k}_1} & 1 \end{bmatrix}$$

and

$$\tilde{Q}_2 = \frac{\tilde{k}_2}{2}\begin{bmatrix} 2\tilde{k}_4 + \tilde{k}_2^2 - 2\delta_2 & -\tilde{k}_2 - 2\frac{\delta_2}{\tilde{k}_1} \\ -\tilde{k}_2 - 2\frac{\delta_2}{\tilde{k}_1} & 1 \end{bmatrix}$$

Note that significant algebraic manipulation is necessary to achieve the structure in (17.62) because although $V(\xi)$ and $\dot{V}(\xi)$ present a decoupled block structure as given in (17.60) and (17.62), the differential equations in (17.56)-(17.59) are coupled. In achieving (17.62) the skew symmetry of the satellite plant and the additional coupling terms have been exploited.

In this situation $\dot{V}(\xi)$ is negative definite if $\tilde{Q}_1$ and $\tilde{Q}_1$ are positive definite. Provided the scalar positive gains $\tilde{k}_i$, for $i = 1,\ldots,4$, satisfy the following conditions

$$\tilde{k}_1 > 0, \quad \tilde{k}_3 > 3\delta_1 + 2\frac{\delta_1^2}{\tilde{k}_1^2} \tag{17.63}$$

$$\tilde{k}_2 > 0, \quad \tilde{k}_4 > 3\delta_2 + 2\frac{\delta_2^2}{\tilde{k}_2^2} \tag{17.64}$$

$\tilde{Q}_1$ and $\tilde{Q}_2$ are positive definite and consequently $\dot{V}(\xi)$ is negative definite for all $\xi \neq 0$ and $t > 0$. Exploiting the very specific block diagonal structure of the Lyapunov matrix in (17.61), rewrite the quadratic Lyapunov function in (17.60) as

$$V(\xi) := \underbrace{\xi_1^{\mathrm{T}}P_1\xi_1}_{V_1(\xi_1)} + \underbrace{\xi_2^{\mathrm{T}}P_2\xi_2}_{V_2(\xi_2)} \tag{17.65}$$

The functions $V_1(\xi_1)$ and $V_2(\xi_2)$ are positive definite with respect to ξ_1 and ξ_2 respectively. Then following identical arguments to those in [[21]], the inequality in (17.62) can be written as

$$\dot{V}(\xi) \leq -\frac{1}{|e_1|^{\frac{1}{2}}}\gamma_{min}(\tilde{Q}_1)\|\xi_1\|_2^2 - \frac{1}{|e_3|^{\frac{1}{2}}}\gamma_{min}(\tilde{Q}_2)\|\xi_2\|_2^2 \tag{17.66}$$

As argued in [[21]], inequality (17.66) can further be written as

$$\dot{V}(\xi) \leq -\beta_1 V_1^{\frac{1}{2}}(\xi_1) - \beta_2 V_2^{\frac{1}{2}}(\xi_2) \tag{17.67}$$

where $\beta_1 = \frac{\gamma_{min}^{\frac{1}{2}}(P_1)\gamma_{min}(\tilde{Q}_1)}{\gamma_{max}(P_1)}$ and $\beta_2 = \frac{\gamma_{min}^{\frac{1}{2}}(P_2)\gamma_{min}(\tilde{Q}_2)}{\gamma_{max}(P_2)}$ and thus it follows that

$$\dot{V}(\xi) \leq -\beta(V_1^{\frac{1}{2}}(\xi_1) + V_2^{\frac{1}{2}}(\xi_2)) \tag{17.68}$$

where $\beta = \min(\beta_1, \beta_2)$. Since $(V_1^{\frac{1}{2}} + V_2^{\frac{1}{2}})^2 > V_1 + V_2$, because V_1 and V_2 are positive, it can be concluded that $V_1^{\frac{1}{2}} + V_2^{\frac{1}{2}} > V^{\frac{1}{2}}$. This further implies that

$$\dot{V}(\xi) \leq -\beta V^{\frac{1}{2}} \tag{17.69}$$

and hence $V(\xi) \equiv 0$ in *finite time*. As argued above, the origin $e = 0$ is attained in *finite time*. Substituting for $e \equiv 0$ in (17.57) and (17.59) yields

$$\underbrace{\tilde{k}_3 \operatorname{sign}(e_1)}_{\nu_1} - f_x = 0 \tag{17.70}$$

$$\underbrace{\tilde{k}_4 \operatorname{sign}(e_3)}_{\nu_3} - f_y = 0 \tag{17.71}$$

Therefore $\nu_{eq,1} := f_x$ and $\nu_{eq,3} := f_y$, where $\nu_{eq,*}$ denotes the equivalent injection signals [[23]] necessary to maintain sliding. Thus f_x and f_y can be obtained to good accuracy by low pass filtering of ν_1 and ν_3 [[23]].

The following simulation shows the filtered injection signals tracking unknown sinusoidal faults/disturbances within the system. Figure 17.5 shows super-twisting-like performance. One the state estimation errors become zero after approximately 3 seconds, tracking of the unknown sinusoidal faults occurs.

17.5 Conclusions

This chapter has presented the application of second order sliding mode observer schemes to the ADDSAFE benchmark problem and a satellite formation flying problem. Two different FDD problems have been considered: firstly the detection and isolation problem associated with an actuator jam/runaway, and secondly an OFC scenario associated with the aileron actuators. Simulation results based on the full nonlinear model of the ADDSAFE aircraft, using a highly detailed model of the right inboard aileron actuator have been carried out. Both liquid and solid OFC cases have been considered. The results show good estimates of both the actuator rod speed and the OFC. A problem associated with fault detection in a formation

flying scenario, associated with satellites has also been discussed. This application to a relative degree two problem would be difficult to solve using linear unknown input observer methods.

References

1. Alwi, H., Edwards, C.: Fault detection and fault-tolerant control of a civil aircraft using a sliding-mode-based scheme. IEEE Transactions on Control Systems Technology 16(3), 499–510 (2008)
2. Alwi, H., Edwards, C.: Oscillatory failure case detection for aircraft using an adaptive sliding mode differentiator scheme. In: American Control Conference, San Francisco, California, USA (2011)
3. Besch, H.M., Giesseler, H.G., Schuller, J.: Impact of electronic flight control system (EFCS) failure cases on structural design loads. Agard report 815, loads and requirements for military aircraft (1996)
4. Dávila, A., Moreno, J.A., Fridman, L.: Variable Gains Super-Twisting Algorithm: A Lyapunov Based Design. In: IEEE American Control Conference, pp. 968–973 (2010)
5. de Jager, B.: Comparison of methods to eliminate chattering and avoid steady state errors in sliding mode digital control. In: Proceedings of the IEEE VSC and Lyapunov Workshop, Sheffield, pp. 37–42 (1992)
6. Edwards, C., Spurgeon, S.K., Patton, R.J.: Sliding mode observers for fault detection. Automatica 36, 541–553 (2000)
7. Fridman, L., Davila, J., Levant, A.: Second-order sliding modes observer for mechanical systems. IEEE Trans. Autom. Control 50, 1785–1789 (2005)
8. Fridman, L., Davila, J., Levant, A.: High-order sliding-mode observation and fault detection. In: Proceedings of the Conference on Decision and Control, New Orleans, U.S.A., pp. 4317–4322 (2007)
9. Fridman, L., Levant, A.: Higher order sliding modes. In: Perruquetti, W., Barbot, J.P. (eds.) Sliding Mode Control in Engineering, pp. 53–96. Marcel Dekker, New York (2002)
10. Goupil, P.: Oscillatory failure case detection in the A380 electrical flight control system by analytical redundancy. Control Engineering Practice 18(9), 1110–1119 (2010)
11. Goupil, P., Marcos, A.: Advanced diagnosis for sustainable flight guidance and control: The european addsafe project. SAE Technical Paper 2011-01-2804 (2011)
12. Goupil, P., Puyou, G.: A high fidelity AIRBUS benchmark for system fault detection and isolation and flight control law clearance. In: European Conference for AeroSpace Sciences (EUCASS 2011) (2011)
13. Hecker, S.: Nominal and faulty LFT/LPV models. ADDSAFE report D1.3.2-3, DLR (2010)
14. Hermans, F.J.J., Zarrop, M.B.: Sliding mode observers for robust sensor monitoring. In: Proceedings of the 13th IFAC World Congress, pp. 211–216 (1996)
15. Jiang, B., Staroswiecki, M., Cocquempot, V.: Fault estimation in nonlinear uncertain systems using robust sliding–mode observers. IEE Proceedings: Control Theory & Applications 151, 29–37 (2004)
16. Kim, Y.W., Rizzoni, G., Utkin, V.: Developing a fault tolerant power train system by integrating the design of control and diagnostics. International Journal of Robust and Nonlinear Control 11, 1095–1114 (2001)
17. Levant, A.: Higher-order sliding modes, differentiation and output-feedback control. International Journal of Control 76(9-10), 924–941 (2003)

18. Luo, N.S., Feng, C.B.: A new method for suppressing chattering in variable structure feedback control systems. In: Nonlinear Control Systems Design: Science Papers of the IFAC Symposium, pp. 279–284. Pergamon, Oxford (1989)
19. Marcos, A.: Advanced fault diagnosis for sustainable flight guidance and control. In: 6th European Aeronautics Days, AERODAYS, Madrid, Spain (2011)
20. Massey, T., Shtessel, Y.: Continuous traditional and high order sliding modes for satelite formation control. AIAA Journal of Guidance Control and Dynamics 28(4), 826–831 (2005)
21. Moreno, J.A., Osorio, M.: A Lyapunov approach to second-order sliding mode controllers and observers. In: 47th IEEE Conference on Decision and Control, pp. 2856–2861 (2008)
22. Tan, C.P., Edwards, C.: Sliding mode observers for robust detection and reconstruction of actuator and sensor faults. International Journal of Robust and Nonlinear Control 13, 443–463 (2003)
23. Utkin, V.I.: Sliding Modes in Control Optimization. Springer, Berlin (1992)
24. Yang, H., Saif, M.: Fault detection in a class of nonlinear systems via adaptive sliding observer. In: Proceedings of the IEEE International Conference on Systems, Man and Cybernetics, pp. 2199–2204 (1995)
25. Yeh, H.H., Nelson, E., Sparks, A.: Nonlinear tracking control for satellite formations. AIAA Journal of Guidance Control and Dynamics 25(2), 376–386 (2002)
26. Young, K.K.D., Drakunov, S.V.: Sliding mode control with chattering reduction. In: Proceedings of the IEEE VSC and Lyapunov Workshop, pp. 188–190 (1992)